Fire Safety Journal 46 (2011) 48–55

Contents lists available at ScienceDirect

Fire Safety Journal

journal homepage: www.elsevier.com/locate/firesaf

Scaling the transport of firebrands by wind-blown plumes

J.L. Consalvi [a,*], P. Mindykowski [a], J.P. Vantelon [b], B. Porterie [a]

[a] Université de Provence, IUSTI/UMR CNRS 6595, 5 rue E. Fermi, 13453 Marseille Cedex 13, France
[b] LCD, UPR 9028 CNRS ENSMA1 Avenue Clément Ader, BP 40109, 86961 Futuroscope Chasseneuil Cedex, France

ARTICLE INFO

Available online 9 September 2010

Keywords:
Firebrands
Transport
Windblow plume
Scaling

ABSTRACT

The possibility of using a reduced-scale model based on the Froude-scaling technique to study the transport of spherical, cylindrical and disk-shaped firebrands by a wind-blown plume was investigated theoretically. The cases of hot particles produced by arcing copper power lines and burning sparks produced by arcing aluminium power lines were also considered. In each case, scaling relationships were derived for mass, linear-momentum, angular momentum and energy transport equations of the firebrands, using well-established models. The analysis shows that, in the case of cylindrical firebrands, incompatible conditions on brand diameter are obtained to scale both the linear-momentum equation and the mass and energy equations. It also shows that all physical processes scale correctly for hot copper particles as well as spherical and disk-shaped burning embers with the exception of the conservation of angular momentum in the case of disks. Despite this drawback, numerical results, obtained using an integral model representing a wind-blown plume, show that the mass and spatial distributions for both types of firebrands can be satisfactorily reproduced down to a scale of 1:5.

1. Introduction

Spotting is the process whereby flaming or burning embers (firebrands) produced when brush and trees burn rapidly are lofted by fire plumes and transported downwind to start new fires (spot fires) in receptive fuel beds, including forests and houses ahead of the main fire. This is an important fire propagation mechanism in high-intensity forest fires. Firebrands (e.g. bark, needles, leaves, cones, and small branches) may give rise to secondary fires hundreds of meters from the fire front and are the primary cause of house ignition in wildland–urban interface areas. Spotting dramatically alters fire growth patterns and behaviour, and makes fire suppression much more difficult. Factors that affect the generation and propagation of firebrands are fuel (size, type, moisture content, and arrangement), weather, and topography. Crown fires can be excellent generators of embers for spotting. Since the capacity of brands to ignite new spot fires depends primarily on their energetic content at landing and on the characteristics of the receptive fuel bed, the first thing required in the modelling of spotting is to study the trajectories and burning rates of the flying embers. The lofting and propagation of burning brands in forest fires have received considerable attention. In their pioneering works, Tarifa et al. [1,2] experimentally determined the drag and burning rates of spheres, cylinders, and plates of certain wood species. These data were used to compute the maximum range of possible fire spread based on terminal fall velocities. Albini [3–6] carried out experiments to determine burning rates for various woods and different geometries and extended the modelling work of Tarifa et al. by considering brands lofted by line thermals and fire plumes. Brand shape effects were studied by Muraszew et al. [7], Woycheese and Pagni [8,9,10], and Anthenien et al. [11]. Muraszew et al. [7] considered spheres, cylinders, and plates lofted in fire whirls, modelling mass loss via an exponential decay of density in connection with Tarifa's mass burning law to determine diameter regression. Woycheese and Pagni [8–10] examined firebrands in the shape of spheres and disks, lofted by a vertical plume, existing as a flow field separate from the horizontal crosswind. Anthenien et al. [11] used a buoyancy-dominated plume model assuming that the horizontal speed is equal to the crosswind speed in order to compare trajectories for spherical, cylindrical, and disk geometries. They found that disks propagate the farthest and have the highest remaining mass fraction at landing. Himoto and Tanaka [12] and Sardoy et al. [13] studied the transport of disk-shaped firebrands, using a *CFD* model to predict plume characteristics. Furthermore, Himoto and Tanaka [12] performed a relevant dimensional analysis to relate the normalized landing distance of brands to a dimensionless scaling parameter, selecting the diameter of the fire source as the characteristic length scale. In their analysis, they assume that non-burning firebrands are released into a vertical McCaffrey plume, neglecting the effects of wind and combustion.

This literature survey indicates that most of the studies concerning the transport of firebrands carried by the wind after

* Corresponding author. Tel.: +33 491 106 927; fax: +33 491 106 969.
E-mail address: Jean-Louis.Consalvi@polytech.univ-mrs.fr (J.L. Consalvi).

0379-7112/$ - see front matter © 2010 Elsevier Ltd. All rights reserved.
doi:10.1016/j.firesaf.2010.07.005

Nomenclature

A_p	projected area
C_D	drag coefficient
C_L	lift coefficient
c_p	specific heat
d	horizontal distance measured from the fire front
D_f	diameter of firebrand
D_{eff}	effective diameter of firebrand
g	gravity acceleration
h	heat transfer coefficient
k	conductivity
L	characteristic length
m_f	mass of firebrand
Pr	Prandtl number
S	scale ratio, (small model size): (large prototype size)
S_f	surface of firebrand
t	time
T	temperature
$\vec{u}_f$	velocity of firebrand
V_f	volume of firebrand
$\vec{w}$	velocity of gas
$\vec{x}_f$	coordinates of firebrand

Greek symbols

ε_f	emissivity of firebrand
μ	viscosity
ν	kinematic viscosity
ρ	density
σ	Stephan Boltzman constant
τ_{f0}	thickness of firebrand
ω_{fz}	spin of firebrand with respect to the z-axis

Subscripts

f	firebrand or fuel particle
film	gas phase near the particle surface
0	initial or reference value
∞	ambient

Superscript

*	dimensionless variable

being lofted by the wind-blown plumes are theoretical. In addition an experimental investigation on a full scale appears to be a very difficult task. The aim of the present approach, which is inspired by the work of Himoto and Tanaka [12], is therefore to investigate the possibility of using a reduced-scale model based on the Froude-scaling technique to study the transport firebrands of different shapes. Previously validated models for firebrand transport and combustion are used to derive the scaling relationships for the transport, combustion, and heat exchange of firebrands. The combustion model, taken from the works of Tse and Fernandez-Pello [14] and Anthenien et al. [11], was validated by comparison with the experimental data of Tarifa et al. [1,2]. Recently [15], the complete model (transport and combustion) was successfully applied to predict the mass and spatial distributions of cylindrical and disk-shaped firebrands obtained experimentally on a large scale by Manzello et al. [16], using a firebrand generator. The transport of hot particles produced by arcing copper power lines and burning sparks produced by arcing aluminium power lines are also considered.

2. Models

2.1. Equations of motion

For simplicity, we consider a 2D flow generated by a wind-blown line fire. Whatever the geometry and burning conditions of firebrands, their motion is governed by the same laws. In this study spherical, cylindrical, and disk geometries are considered. The advection and rotation of the particle are described with the conservation equations of linear-momentum and angular momentum

$$\begin{aligned} \rho_f V_f \frac{d\vec{u}_f}{dt} &= \vec{F}_D + \vec{F}_L + \vec{F}_G \\ I_{fz}\frac{d\omega_{fz}}{dt} &= M_z \end{aligned} \tag{1}$$

$\vec{F}_D$, $\vec{F}_L$ and $\vec{F}_G$ are the drag, lift, and gravitational forces, respectively. I_{fz} and M_Z are the moment of inertia with respect to the z-axis and the torque applied to the particle. The drag, lift, and the gravitational forces can be expressed as follows:

$$\begin{aligned} \vec{F}_D &= \frac{1}{2}\rho_{film} C_D A_p \left|\vec{u}_{\text{rel}}\right| \vec{u}_{\text{rel}}; \\ \vec{F}_L &= \frac{1}{2}\rho_{film} C_L A_p \left|\vec{u}_{\text{rel}}\right|^2 \frac{\vec{u}_{\text{rel}} \times \vec{\omega}_{\text{rel}}}{\left|\vec{u}_{\text{rel}} \times \vec{\omega}_{\text{rel}}\right|}; \\ \vec{F}_G &= \left(\rho_f - \rho_{film}\right) V_f \vec{g} \end{aligned} \tag{2}$$

$\vec{u}_{rel}$ and $\vec{\omega}_{rel}$ are the relative particle/gas velocity and the relative particle/gas vorticity, respectively. Cylinders are assumed to be transported with their axis perpendicular to the relative velocity. For spheres and cylinders, rotation and induced lift forces are neglected. For disk-shaped firebrands, these phenomena have a significant effect on the motion and must be retained. The expressions used to model them will be discussed below. The drag coefficient, C_D, is a function of the Reynolds number defined by $\mathrm{Re} = \left|\vec{u}_{\text{rel}}\right| D_f / \nu_{film}$.

2.1.1. Spheres

For spheres, the drag coefficient relationship is taken from Clift and Gauvin [17]. It has the advantage of being a single relationship for the entire range ($\mathrm{Re} < 3 \times 10^5$) of Reynolds numbers encountered.

$$C_D = \frac{24}{\mathrm{Re}}\left(1 + 0.15\mathrm{Re}^{0.687}\right) + \frac{0.42}{\left(1 + 4.25 \times 10^4 \mathrm{Re}^{-1.16}\right)} \tag{3}$$

2.1.2. Cylinders

The relationship for cylinder drag is taken from Sucker and Brauer [18] and is expected to be accurate over a wide range of Reynolds numbers ($10^{-4} < \mathrm{Re} < 2 \times 10^5$)

$$C_D = 1.18 + \frac{6.8}{\mathrm{Re}^{0.89}} + \frac{1.96}{\mathrm{Re}^{0.5}} - \frac{4 \times 10^{-4}\mathrm{Re}}{1 + 3.64 \times 10^{-7}\mathrm{Re}^2} \tag{4}$$

2.1.3. Disks

The aerodynamic model is taken from [19], in which the trajectory of windborne debris is studied. The rotational moment

exerted on the firebrand induces a continuous change in the orientation of the firebrand and consequently in the magnitude of drag and lift forces. Drag and lift coefficients are functions of the normal coefficient C_N and of the attack angle α

$$C_D = C_N \sin\alpha; C_L = C_N \cos\alpha \tag{5}$$

The normal coefficient is related to the drag coefficient for an attack angle of 90° by the following relationship [20]:

$$C_N = C_{D90} \sin\alpha/(0.56+0.44\sin\alpha) \tag{6}$$

According to Clift et al. [21], C_{D90} can be expressed as a function of the Reynolds number by

$$C_{D90} = \frac{64}{\pi \mathrm{Re}}(1+0.138\mathrm{Re}^{0.792}) \text{ for } \mathrm{Re} \le 130 \text{ and } C_{D90} = 1.17 \text{ for } \mathrm{Re} > 130 \tag{7}$$

The resulting moment acting on the particle, M_z, is due to the non-coincidence of the centres of mass and hydrodynamic forces [19]. It is given by

$$M_z = \frac{1}{2}\rho_{film} C_M A_p D_f |u_{\mathrm{rel}}|^2 \tag{8}$$

where the pitching moment coefficient, C_M, is related to the normal force coefficient, C_N, and to the position of the centre of pressure, x_{cp}

$$C_M = C_N \frac{x_{cp}}{D_f} \tag{9}$$

Holmes et al. [19] have developed a segmented model of x_{cp}/D_p as a function of the angle of attack, which provides the best fit of the available experimental data.

2.2. Equations of heat and mass transfer

2.2.1. Spherical copper particles

Hot copper particles are assumed to be spherical, inert, thermally thin, and released in a solid phase at melting temperature [14]. During their flight paths, they exchange heat with the surrounding medium by convection and radiation.

$$m_f c_{pf} \frac{dT_f}{dt} = -S_f\left[h(T_f - T_\infty) + \varepsilon_f \sigma (T_f^4 - T_\infty^4)\right] \tag{10}$$

The average convection heat transfer coefficient is calculated through the Nusselt number, using the Ranz–Marshall correlation [22]

$$Nu = hD_f/k_{film} = 2 + 0.6\mathrm{Re}^{1/2}\mathrm{Pr}^{1/3} \tag{11}$$

2.2.2. Spherical aluminium particles

In agreement with Tse and Fernandez-Pello [14], the d-square law of droplet combustion is used for the combustion of aluminium particles, which are assumed to be spherical

$$\frac{dD_f^2}{dt} = -K_0(1+0.276\mathrm{Re}^{1/2}\mathrm{Pr}^{1/3}) \tag{12}$$

with $K_0 = 2.8\times10^{-3}$ cm^2/s. During the combustion process, the aluminium particle surface remains at boiling temperature with its surrounding flame at the boiling temperature of aluminium oxide. Extinction is assumed to occur at $Re \ge 138$ and the aluminium particle cools down due to convective and radiative heat transfer to the environment (Eqs. (10) and (11)).

2.2.3. Firebrands

The firebrand combustion model is taken from the works of Tse and Fernandez-Pello [14] and Anthenien et al. [11]. The starting point of the model is that embers can burn heterogeneously (glowing combustion), and thus high Reynolds numbers can enhance their burning without extinction due to flame blow-off. As firebrands burn, they lose mass via both in-depth pyrolysis and surface combustion and their volume decreases as a result of the heterogeneous (glowing) combustion at the outer surface. The model considers that the outer surface of the firebrand is held at a constant temperature and that a pyrolysis front propagates inwards. An effective mass diameter, D_{eff}, is used to capture the location of the pyrolysis front. Based on the data of Tarifa et al. [1,2] a "d-square" law is adopted to describe the regression of D_{eff}, whereas a "d-quarted" law is used to simulate the regression of the actual diameter of the firebrand, D_f. The model depends on a "quiescent atmosphere" burning constant β_0 which, for a given wood species, is found to be independent of both particle shape and wind velocity. Model results were validated against the experimental data of Tarifa et al. [1,2].

- Spheres
  The effective mass diameter D_{eff} decreases as

$$\frac{dD_{eff}^2}{dt} = -\beta_0\left(1+0.276\mathrm{Re}^{1/2}\mathrm{Pr}^{1/3}\right) \tag{13}$$

  where the Frössling relation is used to take into account the increase in the burning rate due to the velocity of the air relative to the particle. The mass of the particle is given by

$$m_f = \frac{\rho_f \pi D_{eff}^3}{6} \tag{14}$$

  The evolution of the diameter of the particle, D_f, is given by

$$\frac{dD_f^4}{dt} = -2\sqrt{3}[\beta_0(1+0.276\mathrm{Re}^{1/2}\mathrm{Pr}^{1/3})]^2 t \tag{15}$$

  Following the previous studies [11], [14], heterogeneous extinction is assumed to occur when $m_f/m_{f0} = 0.24$ as the ember is totally reduced to char (the char yield is assumed to be 0.24 in agreement with Atreya [23]). Upon extinction, the brand is assumed to cool down from an initial temperature of 993 K according to radiative and convective heat transfer processes (Eqs. (10) and (11)).
- Cylinders
  The firebrand combustion model for cylinders is derived from that for spheres by continuing to use Eq. (13) unchanged for the effective diameter, and dividing the right hand side of Eq. (15) by the cylinder aspect ratio $E = \tau_{f0}/D_{f0}$. After the reaction extinguishes, Eq. (10) is used to compute brand temperature and the heat transfer coefficient is calculated from the Nusselt number given by [18]

$$Nu = 0.42\mathrm{Pr}^{0.2} + 0.57\mathrm{Re}^{1/2}\mathrm{Pr}^{1/3} \tag{16}$$

- Disks
  The disks considered here have a small aspect ratio of $\tau_{f0}/D_{f0} \approx O(10^{-2})$. Observations of the burning of such disks suggest that they smoulder radially from the cylindrical periphery to the centre, rather than axially, from one planar face to the opposite face, as observed in disks with a larger aspect ratio [11]. As a consequence, disk thickness τ_{f0} is assumed to remain constant. In addition, it is assumed that, due to the small aspect ratio, char is fragile and breaks off as soon as it is formed [11]. Consequently, char is ignored when the current mass of the firebrand is determined. The mass loss

rate is thus expressed by

$$\frac{dm_f}{dt} = -\frac{\rho_f \pi \tau_{f0}}{4}\frac{d}{dt}\left(\frac{D_f^2}{4}\right) = -\frac{\pi \rho_f \tau_{f0}}{4}\beta_0(1+0.276\mathrm{Re}^{1/2}\mathrm{Pr}^{1/3}) \tag{17}$$

3. Scaling relationships

The wind-blown line plume carrying the firebrands can be reproduced from scale to scale, using Froude modelling [24]. The similitude condition concerning the Froude number requires that velocities scale as

$$U_0 \propto L^{1/2} \tag{18}$$

This implies that the convective heat released rate (CHRR) transported into the plume and the characteristic flow time scale as

$$\dot{Q}'_c \propto L^{3/2}$$
$$t_0 \propto L/U_0 \propto L^{1/2} \tag{19}$$

This section investigates the conditions required for the various characteristic dimensions of the fuel particles to reproduce their flying paths (dynamics, temperature history, and burning) at different scales. In order to address this issue, the following normalized quantities are defined

$$t^* = \frac{t}{t_0}; \quad w^* = \frac{w}{U_0}; \quad x_f^* = \frac{x_f}{L} \tag{20}$$

3.1. Spherical metallic particles and firebrands

3.1.1. Dynamics

The Reynolds number is assumed to be sufficiently high for the drag coefficient to approach its asymptotic limit given in Eq. (3) as

$$C_D = B\mathrm{Re}^{-0.313} \text{ with } \mathrm{Re} = \left|\vec{u}_f - \vec{w}\right| D_f/\nu_{film} \tag{21}$$

In the absence of a significant mass loss due to combustion, the equation of motion of a sphere-shaped firebrand becomes, using the normalized variables defined previously

$$\frac{d^2\vec{x}_f^*}{dt^{*2}} = \frac{t_0^2}{L}\vec{g} - \frac{3\rho\nu_{film}^{-0.687}B}{4\rho_f}\left(\frac{t_0^2 U_0^{1.687}}{L D_f^{1.313}}\right)\left|\frac{L}{t_0 U_0}\frac{d\vec{x}_f^*}{dt^*} - \vec{w}^*\right|^{0.687} \times \left(\frac{L}{t_0 U_0}\frac{d\vec{x}_f^*}{dt^*} - \vec{w}^*\right) \tag{22}$$

Eqs. (18) and (19) imply that t_0^2/L and L/t_0U_0 are constant. It is thus deduced from Eq. (22) that the relative trajectory of an isothermal and non-burning spherical firebrand is reproduced among the different scales provided that

$$D_f \propto L^{0.64} \tag{23}$$

It must be underlined that in addition to this requirement, the initial firebrand velocity must scale with $L^{1/2}$.

3.1.2. Heat transfers

Following the assumptions made in the previous section particles cool down according to Eq. (10), this physical process being subsequent to combustion extinction for aluminium particles and burning embers. The temperature of hot copper particles is normalized using their melting (initial) temperature, whereas that of aluminium particles and embers is normalized using their burning temperature. These reference temperatures are referred to as T_{f0}. Using normalized variables Eq. (10) reduces to

$$\frac{dT_f^*}{dt^*} = -\frac{3.6\mathrm{Pr}^{1/3}k_{film}}{\rho_f \nu_{film}^{1/2} c_{pf}}\left|\frac{L}{t_0 U_0}\frac{d\vec{x}_f^*}{dt^*} - \vec{w}^*\right|^{1/2}\left(T_f^* - T_\infty^*\right) \frac{U_0^{1/2} t_0}{D_f^{3/2}} - \frac{6\varepsilon_f \sigma}{\rho_f c_{pf}} T_{f0}^3\left(T_f^{*4} - T_\infty^{*4}\right)\frac{t_0}{D_f} \tag{24}$$

Consequently, the latter equation is preserved from scale to scale as $t_0 \propto L^{1/2}$, $U_0 \propto L^{1/2}$, and $D_f \propto L^{1/2}$. Comparison with Eq. (23) shows that correct scaling of both dynamics and heat exchange is not obtained. However, since the values of the exponent are close, the discrepancies are not expected to be too large for scales varying within a moderate range. For example, the actual diameter scaled down from $D_f \propto L^{1/2}$ will be smaller than the diameters required to reproduce the equation of motion by a factor $S^{0.14}$, where $S = L_m/L_p$ is the scale ratio. For scale ratios of 1:3, 1:5, and 1:10, this factor is equal to 0.86, 0.8, and 0.72, respectively. In the following it will be assumed that D_{f0} scales with $L^{1/2}$ (see Table 1).

3.1.3. Mass transfers

- Aluminium particles
  The combustion of aluminium particles is described by Eq. (12). Using the assumption of a large Reynolds number, this equation is reduced to:

$$\frac{dD_f^2}{dt} = -0.276K_0\mathrm{Re}^{1/2}\mathrm{Pr}^{1/3} \tag{25}$$

  The diameter of the particle is normalized using its initial value D_{f0}. Using normalized variables, Eq. (25) can be expressed as

$$\frac{dD_f^{*2}}{dt^*} = -0.276K_0\frac{U_0^{1/2}t_0}{D_{f0}^{3/2}}\left[\left|\frac{L}{t_0 U_0}\frac{d\vec{x}_f^*}{dt^*} - \vec{w}^*\right| D_f^*/\nu_{film}\right]^{1/2}\mathrm{Pr}^{1/3} \tag{26}$$

Table 1
Conditions required for scaling dynamics, heat exchange and mass loss of spherical, cylindrical, and disk-shaped firebrands.

Spheres	
Linear-momentum	$D_{f0} \propto L^{0.64}$
Heat exchange	$D_{f0} \propto L^{1/2}$
Mass loss	$D_{f0} \propto L^{1/2}$
Cylinders	
Linear-momentum	$D_{f0} \propto L$
Heat exchange	$D_{f0} \propto L^{1/2}$
Mass loss	$D_{f0} \propto L^{1/2}$
Disks	
Linear-momentum	$\tau_{f0} \propto L$
Angular momentum	$D_{f0} \propto L$
Mass loss	$D_{f0} \propto L^{1/2}$

which is preserved from scale to scale provided that $D_{f0} \propto L^{1/2}$. This scaling relationship is consistent with that obtained for dynamics and heat exchange. Using $D_{f0} \propto L^{1/2}$, the Reynolds number is found to scale with L, which implies that the extinction of aluminium particles cannot be reproduced from scale to scale.

- Firebrands

Firebrand combustion induces mass and diameter reductions during flight. It is fundamental to determine the scaling relationships for mass and diameter reduction and to assess, if they are compatible with $D_{f0} \propto L^{1/2}$. Let us first consider the scaling conditions required for diameter regression. Using the assumption of a high Reynolds number, Eq. (15) reduces to

$$\frac{dD_f^4}{dt} \approx -2\sqrt{3}\left(0.276\beta_0 \mathrm{Re}^{1/2}\mathrm{Pr}^{1/3}\right)^2 t \propto \mathrm{Re}\, t \tag{27}$$

The diameter of the particle is normalized using its initial value D_{f0}. Using normalized variables, Eq. (27) can be expressed as

$$\frac{dD_f^{*4}}{dt^*} \propto \frac{U_0 t_0^2}{D_{f0}^3}\left[D_f^*\left|\frac{L}{U_0 t_0}\frac{dx_f^*}{dt^*} - \vec{w}^*\right|/\nu_{film}\right] t^* \propto \frac{L^{3/2}}{D_{f0}^3} \tag{28}$$

This equation shows that the time evolution of the normalized particle diameter is reproduced from scale to scale provided that $D_{f0} \propto L^{1/2}$.

The scaling relationships concerning mass reduction is now investigated. From Eq. (14), the mass loss rate of a firebrand can be expressed as follows:

$$\frac{dm_f}{dt} = \frac{\rho_f \pi}{2} D_{eff}^2 \frac{dD_{eff}}{dt} \tag{30}$$

From Eq. (13) and on the assumption of a large Reynolds number

$$\frac{dD_{eff}^2}{dt} = -\beta_0\left(1 + 0.276\mathrm{Re}^{1/2}\mathrm{Pr}^{1/3}\right) \approx -0.276\beta_0 \mathrm{Re}^{1/2}\mathrm{Pr}^{1/3} \tag{31}$$

Initially, the effective diameter is equal to the diameter of the particle. The analogy between Eqs. (25) and (31) and the normalization $D_{eff}^* = D_{eff}/D_{f0}$ lead immediately to the scaling relationship $D_{f0} \propto L^{1/2}$. Afterwards, it is easy to normalize Eq. (30), by taking $m_f^* = m_f/m_{f0}$ with $m_{f0} = \pi/6\rho_f D_{f0}^3 \propto L^{3/2}$

$$\frac{dm_f^*}{dt^*} = 3D_{eff}^* \frac{dD_{eff}^{*2}}{dt^*} \tag{32}$$

The latter relationship shows that scaling D_{f0} with $L^{1/2}$ implies that the normalized mass loss rate is conserved from scale to scale.

The analysis above shows that all the physical processes involved in the transport of spherical particles by line plumes scale correctly, except for the extinction of aluminium particles. This is a direct consequence of the dynamic non-similitude of the flow around the spheres resulting from the scaling relationship $\mathrm{Re} = (\rho_{film} U_0 D_{f0}/\mu_{film}) \propto L$. The same dynamic non-similitude of the flow around the particles is present for burning embers. However, the conservation of the relative temperature at different scales requires that two π groups (see Appendix), namely the ratio of the flow time to the thermal response time of the particle, due to convective exchange and the ratio of the flow time to the thermal response time of the particle due to radiative exchange, must be preserved (see Appendix). The conservation of the normalized mass from scale to scale requires that an additional π group, representing the ratio of the burning rate to the mass loss rate of the particle, has to be preserved (see Appendix). This is satisfied provided that $D_{f0} \propto L^{1/2}$.

3.2. Cylindrical and disk-shaped firebrands

The properties of firebrands required to reproduce, at different scales, any physical process involved in the transport of cylindrical and disk-shaped firebrands, are given in Table 1. The derivation of these relationships is based on the assumption of a high Reynolds number, using the same procedure as for spheres. In the case of disk-shaped firebrands, scaling the linear-momentum requires the brand thickness to scale with L. This condition has been used to derive other scaling relationships.

These results show that proper scaling of the transport of both cylindrical and disk-shaped firebrands is not obtained. However, it will be shown that the transport of disk-shaped firebrands can be reproduced up to a reduced scale of 1:10 by scaling the thickness with L and the diameter with $L^{1/2}$.

4. Numerical tests

Table 1 shows that a perfect similitude for both trajectories and heat and mass transfers of burning firebrands does not exist. In addition, the Reynolds number is not conserved among the different scales ($Re \propto L$), which results in a dynamic non-similitude of the flow around the particles. This implies that the assumption of a high Reynolds number, used to derive the scaling relationships, ceases to be valid as the scale reduction becomes too high. The primary aim of this section is to show that despite these drawbacks travelling distances and remaining mass at landing for spherical and disk-shaped firebrands can be reproduced accurately at reduced scales by using the scaling relationships given in Table 2.

Table 2
Summary of scaling relations. Index m refers to 'model' (reduced scale), p to 'prototype' (full scale).

Plume	
Length	$L_m/L_p = S^1$
Time	$t_m/t_p = S^{1/2}$
Speed	$u_m/u_p = S^{1/2}$
Convective heat release rate (CHRR) per unit width	$\dot{Q}'_m/\dot{Q}'_p = S^{3/2}$
Temperature	$\Delta T_m/\Delta T_p = S^0$
Spheres	
Diameter	$D_{f0m}/D_{f0p} = S^{1/2}$
Disks	
Diameter	$D_{f0m}/D_{f0p} = S^{1/2}$
Thickness	$\tau_{f0m}/\tau_{f0p} = S$

Table 3
Summary of fire conditions and firebrand properties at different scales.

Properties	Scale 1	Scale 1:3	Scale 1:5	Scale 1:10
CHRR (MW m^{-1})	22	4.24	1.96	0.69
Wind speed (ms^{-1})	9	5.19	4.02	2.14
Spheres				
D_{f0} (cm)	0.4–3	0.23–1.73	0.18–1.34	0.13–0.95
Disks				
τ_{f0} (mm)	0.1–3	0.033–1	0.02–0.6	0.01–0.3
D_{f0} (cm)	0.4–8	0.23–4.61	0.17–3.6	0.13–2.5

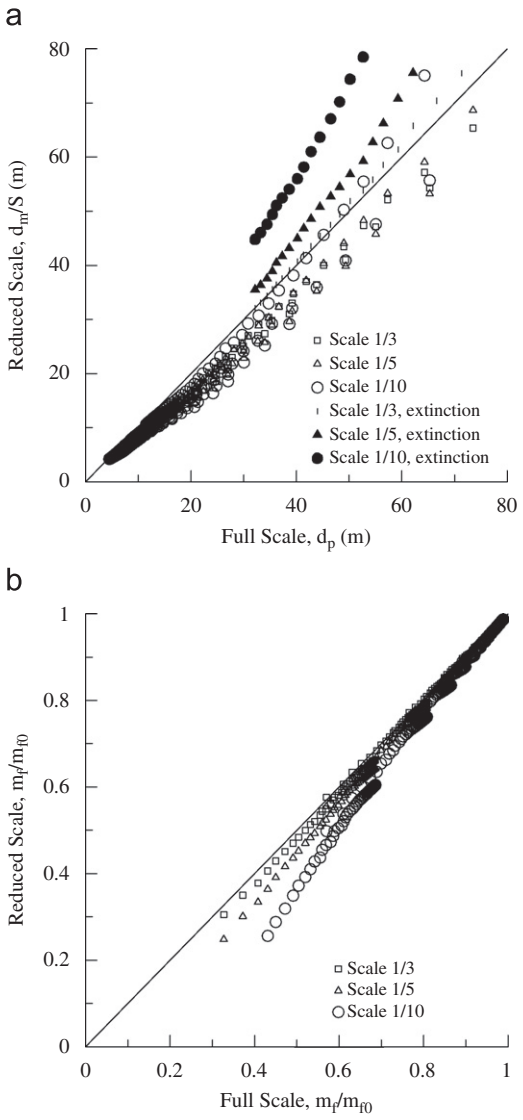

Fig. 1. Spherical firebrands: (a) travelling distance at reduced scale divided by the scale ratio vs. travelling distance obtained at full scale. The extinction label in the legend indicates firebrands that extinguish during their flight. (b) Normalized remaining mass at reduced scale vs. normalized remaining mass at full scale.

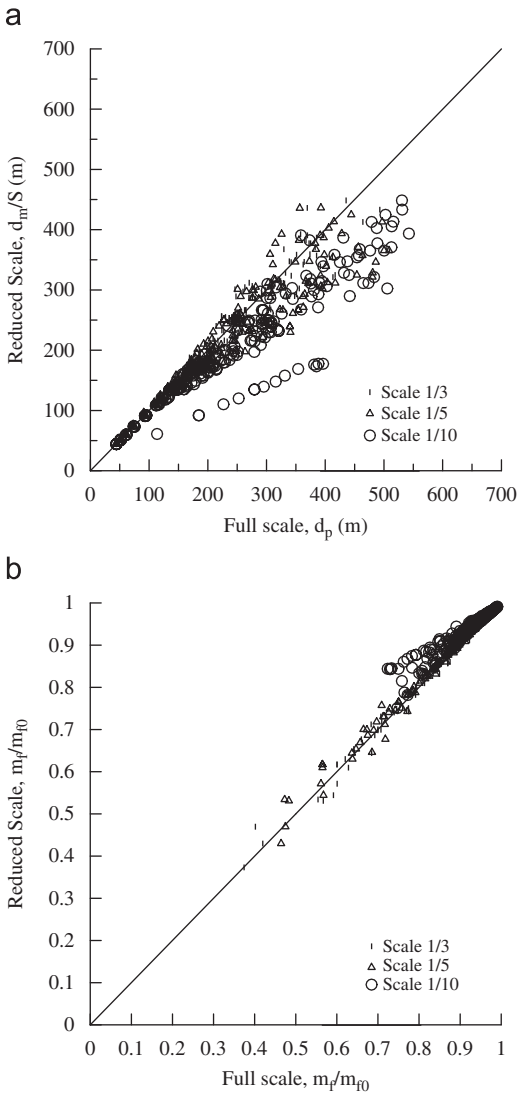

Fig. 2. Disk-shaped firebrands: (a) travelling distance at reduced scale divided by the scale ratio vs. travelling distance obtained at full scale and (b) normalized remaining mass at reduced scale vs. normalized remaining mass at full scale.

Travelling distances and remaining mass at landing are computed at different scales, 1:3, 1:5, and 1:10, by applying the scaling relationships summarized in Table 2 and are compared to those obtained at scale unity. An integral model is used to describe the behaviour of buoyant line plumes released into stratified crossflows. This model is an extension of that of Mercer and Weber [25], in which the top-hat self-similar profile is replaced by a more realistic Gaussian profile. A detailed description of this model can be found in [13]. For each scale, the trajectories of 1000 spherical and disk-shaped firebrands are simulated. Firebrands are released with an initial velocity equal to that of the gas from randomly generated locations along the plume width. Firebrand properties are also generated randomly. Corresponding fire and wind conditions as well as firebrand properties at the different scales are given in Table 3.

Figs. 1 and 2 show a comparison between travelling distances and normalized remaining mass at landing obtained at full and reduced scales for spheres and disk-shaped firebrands, respectively. In Fig. 1a, firebrands that undergo an extinction process during their flight (as they are completely reduced to char) are distinguished from those that reach the ground still burning. Trajectories of spherical firebrands are correctly reproduced at small scales although discrepancies appear at the scale of 1:10, especially for firebrands that extinguish during their flight. The reasons for these discrepancies are stated above, i.e. non-perfect similitude for both trajectories and heat and mass transfers and the dynamic non-similitude of the flow around the particle.

In the case of disk-shaped firebrands, the incorrect scaling of angular momentum does not seem to have a significant effect up to the reduced scale of 1:5. Despite discrepancies an overall agreement is obtained at the reduced scale of 1:10.

5. Conclusions

It is clear that the considered phenomena occur at a scale which precludes all experimental study. Nevertheless, the present work suggests that scale technique based on Froude modelling can be used to investigate the transport of hot particles produced by arcing copper lines and spherical and disk-shaped firebrands by wind-blown line plumes. As often in scaling approaches, all of the variables of the problem cannot be addressed, but the relevant dimensionless groups

have been identified and it has been shown that the scaling technique is proper. A practical application of this technique could be the prediction of safety distances in realistic situations.

Acknowledgments

This work was supported by the ANR PIF under Grant no. NT05–4441.

Appendix: other derivations of the scaling relationships

The following normalized quantities are defined

$$t^*=\frac{t}{t_0};\quad w^*=\frac{w}{U_0};\quad x_f^*=\frac{x_f}{L} \tag{A1}$$

and the following relationships (based on the similitude condition for the Froude number) will be used

$$U_0\propto L^{1/2};\quad t_0\propto L/U_0\propto L^{1/2} \tag{A2}$$

I **Momentum equation**

The linear-momentum equation (Eq. (1) of the main text) can be rewritten as follows:

$$\frac{d^2\vec{x}_f}{dt^2}=\vec{g}+\left(\frac{\vec{u}_f-\vec{w}}{\tau_v}\right) \tag{A3}$$

where $\tau_v=4\rho_f D_f^2/3\mu_{film}C_D\mathrm{Re}$ is the momentum response time of the particle. Using the normalized variables defined by Eqs. (A1), (A3) becomes

$$\frac{d^2\vec{x}_f^*}{dt^{*2}}=\frac{t_0^2\vec{g}}{L}+\frac{t_0}{\tau_v}(\vec{u}_f^*-\vec{w}^*) \tag{A4}$$

Two dimensionless groups appear in the latter equation: $\Pi_1=t_0^2\vec{g}/L$, which represents the ratio of the gravitational acceleration to the acceleration of the flow and the Stokes number, $\Pi_2=t_0/\tau_v$, which represents the ratio of the flow time to the momentum response time of the particle. From Eq. (A2), it appears clearly that $\Pi_1=\mathrm{const}$. By using $C_D=B\mathrm{Re}^{-0.313}$ and $\mathrm{Re}=\left|\vec{u}_f-\vec{w}\right|D_f/\nu_{film}$, it can be seen directly that the condition $\Pi_2=\mathrm{const}$ requires that $D_{f0}\propto L^{0.64}$.

II Energy equation

The energy equation (Eq. (10) of the main test) can be rewritten as

$$\frac{dT_f}{dt}=-\frac{6k_{film}Nu}{\rho_f c_{pf}D_f^2}(T_f-T_\infty)-\frac{6\varepsilon_f\sigma}{\rho_f c_{pf}D_f}(T_f^4-T_\infty^4) \tag{A5}$$

Using the normalized variables defined by Eq. (A1) and normalizing the firebrand temperature by the ambient temperature, we find

$$\frac{dT_f^*}{dt^*}=-\frac{t_0}{\tau_{Tc}}(T_f^*-T_\infty^*)-\frac{t_0}{\tau_{Tr}}(T_f^{*4}-T_\infty^{*4}) \tag{A6}$$

where $\tau_{Tc}=\rho_f c_{pf}D_f^2/6k_{film}Nu$ and $\tau_{Tr}=\rho_f c_{pf}D_f/6\varepsilon_f\sigma T_\infty^3$ represent the thermal response times of the particle due to convective and radiative exchange, respectively. This introduces two additional π groups, $\Pi_3=t_0/\tau_{Tc}$ and $\Pi_4=t_0/\tau_{Tr}$, which represent the ratios of the flow time to these response times. By using the high Reynolds approximation ($\mathrm{Nu}\sim 0.6\mathrm{Re}^{1/2}\mathrm{Pr}^{1/3}$) and Eq. (A2), the condition $\Pi_3=\mathrm{const}$ is obtained provided that $D_{f0}\propto L^{1/2}$. From Eq. (A2), it can be seen directly that the same scaling relationship ($D_{f0}\propto L^{1/2}$) is required to preserve Π_4.

III **Mass and diameter equations**

- Aluminium particles

  The mass loss equation for an aluminium particle is similar to that of an evaporating droplet

$$\frac{dm_f}{dt}=-\dot{m}_b \tag{A7}$$

  where $\dot{m}_b=\frac{\pi}{4}\rho_f D_f K_0(1+0.276\mathrm{Re}^{1/2}\mathrm{Pr}^{1/3})$ is the burning rate of the particle. Normalizing the mass of the particle by its initial mass, and using the normalized variables given by Eq. (A2), we find

$$\frac{dm_f^*}{dt^*}=-\frac{\dot{m}_b t_0}{m_{f0}}=-\Pi_5 \tag{A8}$$

  Π_5 represents the ratio of the burning rate to the mass loss rate of the particle. For high Reynolds numbers and on the basis of Eq. (A2), $\Pi_5\propto(L^{3/4}/D_{f0}^{3/2})$ and is preserved from scale to scale provided that $D_{f0}\propto L^{1/2}$.

- Firebrands
  - The analogy between Eq. (A7) and the mass loss equation of firebrands (Eqs. (13) and (14) of the main test) implies that the same condition ($D_{f0}\propto L^{1/2}$) is required to preserve the relative mass of the firebrand at different scales.
  - Let us finally consider the required scaling conditions for the regression of the diameter. Using the high Reynolds assumption, Eq. (15) (of the main text) reduces to

$$\frac{dD_f^4}{dt}\approx -2\sqrt{3}(0.276\beta_0\mathrm{Re}^{1/2}\mathrm{Pr}^{1/3})^2\,t\propto \mathrm{Re}\,t \tag{A9}$$

  The diameter of the particle is normalized using its initial value D_{f0}. Using normalized variables, Eq. (A9) can be expressed as

$$\frac{dD_f^{*4}}{dt^*}\propto\frac{U_0t_0^2}{D_{f0}^3}\left[D_f^*\left|\frac{L}{U_0t_0}\frac{dx_f^*}{dt^*}-\vec{w}^*\right|/\nu_{film}\right]t^*\propto\frac{L^{3/2}}{D_{f0}^3} \tag{A10}$$

  This equation shows that the time evolution of the normalized particle diameter is reproduced from scale to scale provided that $D_{f0}\propto L^{1/2}$.

References

[1] C.S. Tarifa, P.P.Del Notario, F.G. Moreno, On the flight paths and lifetimes of burning particles of wood, Proc. Combust. Inst. 10 (1965) 1021–1037.
[2] C.S. Tarifa, P.P. Del Notario, F.G. Moreno, A.R. Villa, Transport and combustion of firebrands, final report of grants FG-SP-11 and FG-SP-146, US Dep. Agric. For. Serv. (1967).
[3] F.A. Albini, Spot fire distance from burning trees—a predictive model, general technical report INT-56, USDA For. Serv. (1979).
[4] F.A. Albini, Spot fire distance from isolated sources—extensions of a predictive model, general technical report INT-309, USDA For. Serv. (1981).
[5] F.A. Albini, Potential spotting distance from wind-driven surface fires, research paper INT-309, USDA For. Serv. (1983).
[6] F.A. Albini, Transport of firebrands by line thermals, Combust. Sci. Technol. 32 (1983) 277–288.
[7] A. Muraszew, J.B. Fedele, W.C. Kuby, Trajectory of firebrands in and out of fire whirls, Combust. Flame 30 (1970) 321–324.
[8] J.P. Woycheese, P.J. Pagni, D. Liepman, Brand lofting above large-scale fires, in: Proceedings of the Second International Conference on Fire Research and Engineering, Boston, USA, 1998.
[9] J.P. Woycheese, P.J. Pagni, Combustion models for wooden brands, in: Proceedings of the Third International Conference on Fire Research and Engineering, Boston, USA, 1998.
[10] J.P. Woycheese, P.J. Pagni, D. Liepman, Brand propagation from large-scale fires, J. Fire Prot. Eng. 10 (1999) 32–44.

[11] R.A. Anthenien, S.D. Tse, A.C. Fernandez-Pello, On the trajectories of embers initially elevated or lofted by small scale ground fire plumes in high winds, Fire Saf. J. 41 (2006) 349–363.
[12] K. Himoto, T. Tanaka, Transport of disk-shaped firebrands in a turbulent boundary layer, in: Proceedings of the Eighth International Symposium on Fire Safety Science, 2005, pp. 433–444.
[13] N. Sardoy, J.L. Consalvi, B. Porterie, A.C. Fernandez-Pello, Modeling transport and combustion of firebrands from burning trees, Combust. Flame 150 (2007) 151–169.
[14] S.D. Tse, A.C. Fernandez-Pello, On the flight paths of metal particles and embers generated by power lines in high winds—a potential source of wildland fires, Fire Saf. J. 30 (1998) 333–356.
[15] S. Kortas, P. Mindykowski, J.L. Consalvi, H. Mhiri, B. Porterie, Experimental validation of a numerical model for the transport of firebrands, Fire Saf. J. 44 (2009) 1095–1102.
[16] S.L. Manzello, J.R. Shields, T.G. Cleary, A. Maranghides, W.E. Mell, J.C. Yang, Y. Hayashi, D. Nii, T. Kurita, On the development and characterization of a firebrand generator, Fire Saf. J. 43 (2008) 258–268.
[17] H. Clift, W.H. Gauvin, The motion of particles in turbulent gas streams, Proc. Chemeca 70 (1970) 1–7.
[18] F.M. White, in: Viscous Fluid Flow, second ed., McGraw-Hill, Boston, MA, 1991.
[19] J.D. Holmes, C.W. Letchford, N. Lin, Investigations of plate-type windborne debris—Part II: computed trajectories, J. Wind Eng. Ind. Aerodyn. 94 (2000) 21–39.
[20] C. Lindenburg, Stall coefficients, aerodynamic airfoil coefficients at large angles of attack, in: Proceedings of the IAE symposium on the Aerodynamics of Wind Turbines, ECNRX-01-004, NREL, USA, 2000.
[21] R. Clift, J.R. Grace, M.E. Weber, in: Bubbles, Drops, and Particles, Academic Press. Inc., New York, 1978.
[22] W.E. Ranz, W.R. Marshall, Evaporation from drops—I and II, Chem. Eng. Prog. 48 (1952) 141–180.
[23] A. Atreya, Pyrolysis, ignition and fire spread on horizontal surfaces of wood, Ph.D. Thesis, Harvard University, Cambridge, 1983.
[24] G. Heskestad, Scaling the interaction of water sprays and flames, Fire Saf. J. 37 (2002) 535–548.
[25] G.N. Mercer, R.O. Weber, The plume above a line fire in a wind, Int. J. Wildland Fire 4 (1994) 201–207.